




Article

Carbon Dots versus Nano-Carbon/Organic Hybrids—Divergence between Optical Properties and Photoinduced Antimicrobial Activities

Audrey F. Adcock¹, Ping Wang², Elton Y. Cao³, Lin Ge², Yongan Tang⁴, Isaiah S. Ferguson¹, Fares S. Abu Sweilem¹, Lauren Petta², William Cannon², Liju Yang^{1,*} , Christopher E. Bunker^{3,*} and Ya-Ping Sun^{2,*}

¹ Department of Pharmaceutical Sciences, Biomanufacturing Research Institute and Technology Enterprise, North Carolina Central University, Durham, NC 27707, USA

² Department of Chemistry, Clemson University, Clemson, SC 29634, USA

³ Air Force Research Laboratory, Propulsion Directorate, Wright-Patterson Air Force Base, Dayton, OH 45433, USA

⁴ Department of Mathematics and Physics, North Carolina Central University, Durham, NC 27707, USA

* Correspondence: lyang@ncsu.edu (L.Y.); christopher.bunker@us.af.mil (C.E.B.); syaping@clemson.edu (Y.-P.S.)

Abstract: Carbon dots (CDots) are generally defined as small-carbon nanoparticles with surface organic functionalization and their classical synthesis is literally the functionalization of preexisting carbon nanoparticles. Other than these “classically defined CDots”, however, the majority of the dot samples reported in the literature were prepared by thermal carbonization of organic precursors in mostly “one-pot” processing. In this work, thermal processing of the selected precursors intended for carbonization was performed with conditions of 200 °C for 3 h, 330 °C for 6 h, and heating by microwave irradiation, yielding samples denoted as CS200, CS330, and CS_{MT}, respectively. These samples are structurally different from the classical CDots and should be considered as “nano-carbon/organic hybrids”. Their optical spectroscopic properties were found comparable to those of the classical CDots, but very different in the related photoinduced antibacterial activities. Mechanistic origins of the divergence were explored, with the results suggesting major factors associated with the structural and morphological characteristics of the hybrids.

Keywords: carbon dots; nano-carbon/organic hybrids; thermal carbonization; optical spectroscopy; photoinduced antibacterial



Citation: Adcock, A.F.; Wang, P.; Cao, E.Y.; Ge, L.; Tang, Y.; Ferguson, I.S.; Abu Sweilem, F.S.; Petta, L.; Cannon, W.; Yang, L.; et al. Carbon Dots versus Nano-Carbon/Organic Hybrids—Divergence between Optical Properties and Photoinduced Antimicrobial Activities. *C* **2022**, *8*, 54. <https://doi.org/10.3390/c8040054>

Academic Editors: Olena Okhay and Gil Goncalves

Received: 8 September 2022

Accepted: 17 October 2022

Published: 20 October 2022

Publisher’s Note: MDPI stays neutral with regard to jurisdictional claims in published maps and institutional affiliations.



Copyright: © 2022 by the authors. Licensee MDPI, Basel, Switzerland. This article is an open access article distributed under the terms and conditions of the Creative Commons Attribution (CC BY) license (<https://creativecommons.org/licenses/by/4.0/>).

1. Introduction

Small-carbon nanoparticles, mostly amorphous without defined crystal structures, have suddenly attracted significant attention as a newly “discovered” class of carbon nanomaterials, even with an edge over the pretty fullerene molecules in the competition for the title of carbon at zero dimension in the family of nanoscale carbon allotropes [1]. The fortune of these otherwise ugly nanoparticles is credited to their spectacularly enhanced optical properties upon the effective nanoparticle surface passivation by organic functionalization, namely the formation of carbon “quantum” dots or, more appropriately, carbon dots, due to the lack of any evidence for the classical quantum confinement in small-carbon nanoparticles [1–3]. Carbon dots of such a structural configuration (Figure 1) are commonly referred to as classically defined carbon dots, often denoted as CDots, from the preparation considered as the “top-down” method. In CDots, the photoexcited state properties and redox characteristics are attributed to the effective passivation and stabilization of the abundant surface defect sites on small-carbon nanoparticles via organic functionalization [1,4]. However, despite the rather simple structure of the classically defined CDots and their straightforward synthesis, the rapidly expanding research community relevant to these

nanomaterials has apparently decided that the simple surface functionalization of pre-existing small-carbon nanoparticles is not facile enough, opting instead for the “bottom-up” carbonization approach, with the thermal processing of organic precursors to produce dot samples in “one-pot” [1,5–19]. The implicit assumption for the approach must be such that organic precursors could be thermally carbonized into nanostructures analogous to that of the classically defined CDots (Figure 1) [19], though there has been a general lack of any serious efforts on the nanoscale structural elucidation of the samples produced by the thermal carbonization, let alone any concrete experimental evidence for the validation of the implicit assumption.

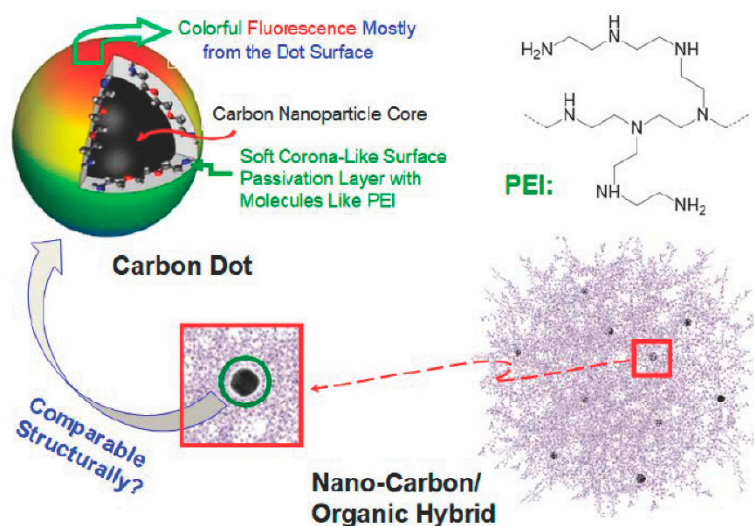


Figure 1. Carbon dots (PEI-CDots as a specific example, classically defined and prepared by the functionalization of preexisting small-carbon nanoparticles with PEI molecules) versus the nanocarbon/organic hybrids from the thermal processing of selected organic precursors.

Among popular organic precursors for the carbonization approach are mixtures of citric acid (CA) with oligomeric polyethylenimine (PEI) [20–26]. The “classical” thermal processing conditions for the CA-PEI precursor mixtures, similar to those for most other organic precursors, are thermal or hydrothermal treatments at temperatures up to 200 °C for a few hours.

The attraction of such an extremely user-friendly synthetic approach is obvious, though the chemical and nanoscale structures of the samples, thus prepared, are most likely very different from those of CDots (Figure 1) [27,28]. There is growing experimental evidence suggesting that the commonly employed processing conditions are generally insufficient for the intended carbonization, yielding samples of little nanoscale carbon (non-molecular carbon) and abundant organic species, often vulnerable to the sample contamination or even spectroscopic dominance by the molecular dyes/chromophores produced in the thermally induced chemical reactions [29–34]. In the much-less-popular synthesis, with more vigorous processing conditions, such as higher temperatures coupled with longer treatment times, more nanoscale carbon contents in the resulting samples could be achieved [27], though the sample structures are likely crosslinked mixtures of the nanoscale carbon with a significant amount of organic species, thus, more appropriately characterized as “nano-carbon/organic hybrids” (Figure 1) [19,28]. It may be further extrapolated that in such sample structures, there are local areas of nano-carbon domains passivated by the surrounding organic species, thus, a structural configuration analogous to that of classically defined CDots (Figure 1), which may account for their observed similar optical spectroscopic features [19].

In this work, the samples from thermal processing of the CA-PEI precursor mixture under different conditions, including hydrothermal at 200 °C and 330 °C and heating by microwave irradiation, were compared among themselves and with PEI-CDots (classically defined CDots of PEI-functionalized preexisting small-carbon nanoparticles) for their

optical spectroscopic properties and photoinduced antimicrobial activities. The results show major divergence, such that there are significant similarities among the samples in optical spectroscopic properties, but their visible-light activated antibacterial activities are very different. Possible structural and mechanistic origins of the divergence are explored and implications of the different structures of the carbonization produced samples from those of the classically defined CDots are discussed.

2. Experimental Section

2.1. Materials

Citric acid was purchased from Alfa Aesar (Tewksbury, MA, USA), oligomeric polyethylenimine (PEI, branched, average molecular weight ~600) from Polysciences, Inc. (Warrington, PA, USA) and *N,N*-diethylaniline and 2,4-dinitrotoluene from Sigma-Aldrich. Dialysis membrane tubing (molecular weight cut-off ~500 or ~1000) was supplied by Spectrum Laboratories. Water was deionized and purified by being passed through a Labconco WaterPros water purification system (Labconco, Kansas City, MO, USA).

2.2. Measurement

UV/vis absorption spectra were recorded on Shimadzu UV2501 and UV-3600 spectrophotometers (Shimadzu Scientific Instruments, Inc., Columbia, MD, USA). Fluorescence spectra were measured on a Jobin-Yvon emission spectrometer equipped with a 450 W xenon source, Gemini-180 excitation and Triax-550 emission monochromators, and a photon-counting detector (Hamamatsu R928P PMT at 950 V) (Hamamatsu Photonics, Bridgewater Township, NJ, USA). Atomic force microscopy (AFM) images were acquired using a Nanosurf CoreAFM instrument (Liestal, Switzerland). Sample specimens for AFM were prepared on clean Si wafer pieces, with blank images obtained under the same conditions using the same Si wafers.

2.3. CS200 Sample

Citric acid (1 g) and PEI (0.5 g) were mixed in water (10 mL) and the resulting mixture was loaded into a stainless-steel tube reactor. The reactor was sealed for heating in a tube furnace at 200 °C for 3 h. Then, the reactor was cooled back to ambient and the reaction mixture in the reactor was collected. The mixture was placed in a membrane tubing (molecular weight cut-off ~1000) for dialysis against fresh water, followed by concentration. A light-brown aqueous solution was obtained as the sample from the carbonization synthesis at 200 °C, denoted as CS200.

2.4. CS330 Sample

Citric acid (1 g) was dissolved in water (2 mL) with brief sonication and the resulting solution was mixed well with PEI (0.5 g). Then, the mixture was loaded into a stainless-steel tube reactor. The reactor was sealed for heating in a tube furnace at 330 °C for 6 h. Upon the cooling of the reactor back to ambient temperature, the reaction mixture in the reactor was collected by washing with water. The aqueous mixture was placed in a membrane tubing (molecular weight cut-off ~1000) for dialysis against fresh water. Upon concentration and then centrifugation, the colored supernatant was collected as the sample from the carbonization synthesis at 330 °C, denoted as CS330.

2.5. CS_{MT} Sample

CA (1 g) in water (2 mL) was mixed well with PEI (3 g), followed by evaporation to remove water for a solid-like mixture. Separately, a bath of silicon carbide (150 g) in a silica crucible casting dish (about 8 cm in diameter and 2.5 cm in height) was prepared and pre-heated in a conventional microwave oven at 500 W for 3 min. The solid-like mixture of CA-PEI in a scintillation vial was immersed in the pre-heated silicon carbide bath for treatments with microwave irradiation, first at 200 W for ~4 min until no more bubbles in the sample and with the sample color turning dark orange and then 1000 W

for 3 min, during which there were 5 brief pauses each of a few seconds. Post-treatment, the reaction mixture was cooled to ambient temperature and dispersed in deionized water with sonication. The resulting aqueous dispersion was centrifuged at $5000\times g$ to keep the supernatant, followed by dialysis in a membrane tubing (molecular weight cut-off ~ 1000) against fresh water to obtain a colored aqueous solution of the sample denoted as CS_{MT}.

2.6. PEI-CDots

Details on the preparation and characterization of PEI-CDots were reported previously [35,36]. Copies of the synthesis protocol and results with references are provided as Supplementary Materials.

2.7. Antibacterial Evaluations

Listeria monocytogenes 10403S cells were used as the target bacteria for evaluations on photoinduced antibacterial activities of the PEI/CA samples and PEI-CDots. *L. monocytogenes* cells were grown in 10 mL brain heart infusion (BHI) by inoculating with a single colony streaked on BHI plate at 37 °C overnight with constant agitation at 225 rpm in an Excella E24 incubator shaker (New Brunswick Scientific, Edison, NJ, USA). The cells were centrifuged in an Eppendorf 5424 microcentrifuge at $4000\times g$ for 5 min and then washed twice with phosphate-buffer saline (PBS). The cell pellet was re-suspended in PBS and diluted to the desired cell concentration for further experiments.

Treatments of the cells with the PEI/CA samples and PEI-CDots were performed in 96-well plates. Aliquots of 100 μ L of bacteria cell suspensions were placed into the wells and 100 μ L of aqueous solutions of the PEI/CA samples and PEI-CDots in various concentrations were added to reach the desired final concentrations for treating the cells. The bacterial cell concentration in each well was in the order of 10^8 CFU/mL. The control samples were bacterial suspension with PBS. The samples for each treatment were duplicated in each experiment. The plates were placed on orbital shaker (BT Lab Systems) at 350 rpm, with exposure to visible light from a commercial 8 W daylight LED lamp (CREE, omnidirectional 815 lumens) placed at a distance of ~ 10 cm away from the plate surface (the light intensity of ~ 4.8 mW/cm² experienced by the samples) for 1 h. For all treatment experiments, at least three independent experiments were performed.

After the treatments, the viable cell numbers in the treated and the control samples were determined using the traditional surface plating method. Briefly, the samples were 1:10 serially diluted with PBS and aliquots of 100 μ L of appropriate dilutions were surface plated on BHI agar plates. The plates were incubated at 37 °C overnight and the colonies were counted and calculated in colony-forming units per mL (CFU/mL) for the viable cell numbers in the samples. The reductions in logarithmic viable cell number in the treated samples comparing to the control samples were used as the measures for the photoinduced antibacterial effects of the PEI/CA samples and PEI-CDots at a given concentration.

3. Results and Discussion

As reported previously [27], the precursor mixture of citric acid (CA) and oligomeric polyethylenimine (PEI) was used for the thermal processing intended for carbonization, thus, the popular “bottom-up” approach for dot samples [1,5–19]. The processing included the heating with the presence of water in a sealed reactor at 200 °C for 3 h and 330 °C for 6 h to obtain the PEI/CA samples denoted as CS200 and CS330 (with CS referring to “carbonization synthesis”), respectively. The same precursor mixture was also processed by more efficient heating via microwave irradiation, again intended for carbonization, yielding the PEI/CA carbonization product denoted as CS_{MT} (with MT referring to “microwave thermal”). For comparison, the classically defined CDot sample PEI-CDots was prepared by using preexisting small-carbon nanoparticles for surface functionalization with PEI molecules, as previously reported [35,36]. All these samples were cleaned post-synthesis to remove residual precursors and other impurities.

On the comparison of optical absorption spectra of the different samples in aqueous solutions (Figure 2), CS200 is only weakly absorptive in visible light (400 nm and longer wavelengths), obviously much weaker than CS330 at comparable sample solution concentrations, consistent with the conclusion that the thermal processing conditions for CS200 are much too mild for the intended substantial carbonization of the precursor mixture [27,28]. However, largely similar are their fluorescence spectral profiles for 400 nm excitation (Figure 2), where the optical absorptions for the excitation of both samples must be due to the nano-carbon domains produced as a result of the carbonization. In fact, the spectral similarity between the fluorescence emissions of these samples and that of PEI-CDots (Figure 2) may also support the more generalized notion that the nano-carbon domains in carbonization-produced samples responsible for the observed optical spectroscopic properties are probably somewhat comparable in structure and morphology to the preexisting small-carbon nanoparticles in classically defined CDots [19], such as PEI-CDots here.

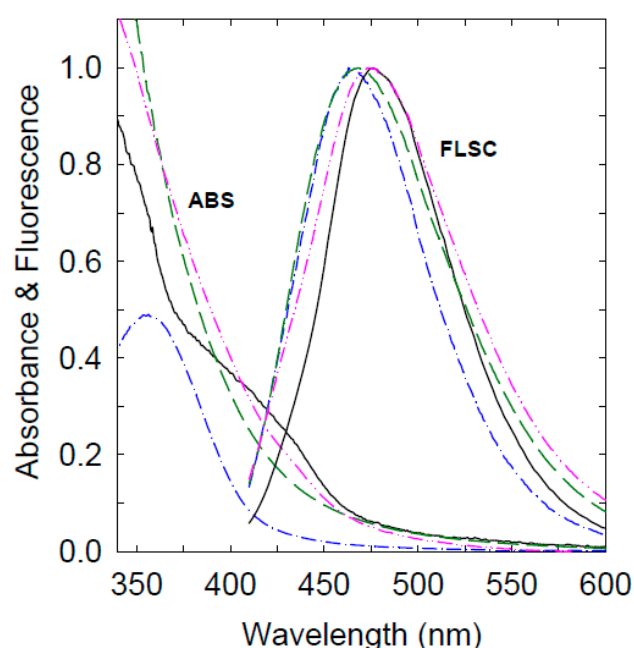


Figure 2. Optical absorption (ABS) and fluorescence (FLSC, 400 nm excitation) spectra of CS200 (dash-dot line), CS330 (solid line), CS_{MT} (dash-dot-dot line), and PEI-CDots (dash line), all in aqueous solutions.

The absorption and fluorescence emission spectra of the CS_{MT} sample in aqueous solution are similar to those of CS330 (Figure 2), for which one may rationalize, such that the microwave irradiation is known for highly efficient heating to result in carbonization of the CA-PEI precursor mixture, comparable to that by thermal processing at high temperatures and/or for longer time periods. If only the optical spectroscopic properties are targeted, one may even argue that the microwave processing should be the method of choice in the carbonization synthesis of dot samples. Interestingly and surprisingly, however, there are major differences between CS330 and CS_{MT} in their other photoexcited state properties and processes or in the consequences of such properties and processes, specifically with respect to the photoinduced antimicrobial function [37,38].

It is known that PEI-CDots with exposure to visible light are effective and efficient in the inactivation of various model bacteria and bacterial pathogens [39,40]. In this work, the three PEI/CA samples (CS200, CS330, and CS_{MT}) were evaluated for visible-light-activated antibacterial activities against *L. monocytogenes*, in reference to those of PEI-CDots. In the evaluation, *L. monocytogenes* cells in PBS suspensions ($\sim 10^8$ CFU/mL) were treated with CS200, CS330, CS_{MT}, and PEI-CDots in different concentrations and all with the visible-light exposure for 1 h, except for the dark controls. After the treatments, the viable cell numbers

in the treated samples and the control samples were determined. The dose–response curve for *L. monocytogenes* in response to each of the tested dot samples is plotted in Figure 3 in terms of the observed logarithmic viable cell numbers against the concentrations of the individual PEI/CA samples and PEI-CDots used in the treatments.

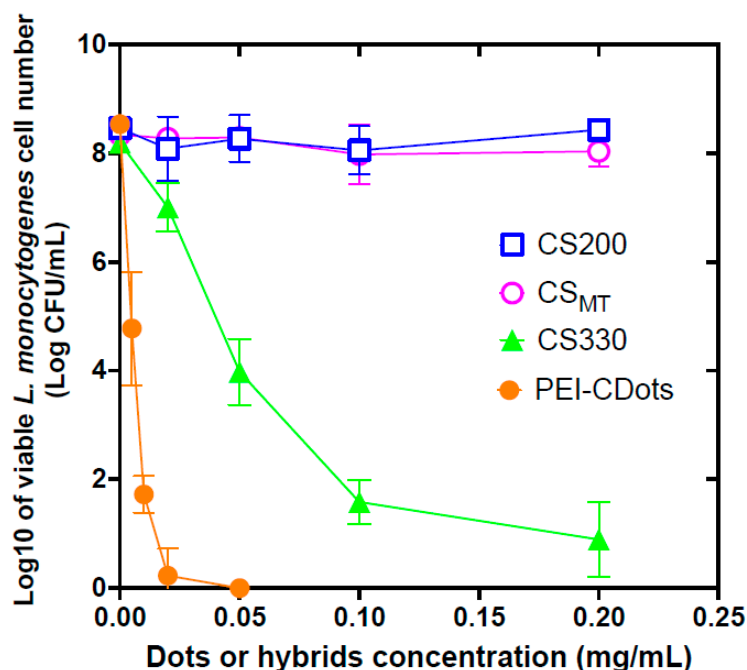


Figure 3. The antibacterial activities of CS200, CS330, CS_{MT}, and PEI-CDots with visible-light exposure (all for 1 h) against *L. monocytogenes* cells, expressed by the reduction in logarithmic viable cell number with increasing concentrations of the hybrids and PEI-CDots.

The CS200 sample clearly lacks the light-activated antibacterial function (Figure 3), which one might argue should be expected for the low content of nano-carbon domains in the sample due to insufficient carbonization, associated with the much-too-mild thermal processing conditions. The more appropriately carbonization-produced CS330 sample with the same visible-light exposure could inactivate *L. monocytogenes* significantly, though still much less effective than PEI-CDots (Figure 3). For the CS_{MT} sample, however, even with its microwave-assisted thermal processing conditions designed for sufficient carbonization and its similar optical spectroscopic properties to those of CS330, its lack of any meaningful antibacterial action, the same as that of the CS200 sample (Figure 3), is really unexpected and striking, suggesting that there are other major factors beyond the content of nano-carbon domains, such as the structural details and/or morphological characteristics of the sample, determining the photoinduced antimicrobial properties.

On the origin of the striking difference between CS330 and CS_{MT} samples in their photoinduced antibacterial activities, photoexcited state properties of the two samples were compared, including the excitation-wavelength-dependent fluorescence emissions and the fluorescence quenching by known electron donor and acceptor molecules, *N,N*-diethylaniline (DEA) and 2,4-dinitrotoluene (DNT), respectively. The electron transfer quenching of fluorescence emissions provides insight into the photoinduced redox processes in the PEI/CA samples, thus, more directly relevant to the photoinduced antibacterial function. As compared in Figure 4, the characteristic excitation wavelength dependence of fluorescence emissions, as generally found in classically defined CDots [41], is apparently similar between CS330 and CS_{MT} samples. Further, also similar between the two samples are the results from redox quenching of fluorescence emissions with electron donor DEA (Figure 5) and acceptor DNT as quenchers (Figure 6) [34,41,42], suggesting no major differ-

ences in the photoexcited state redox characteristics that might account for the strikingly different antibacterial outcomes (Figure 3).

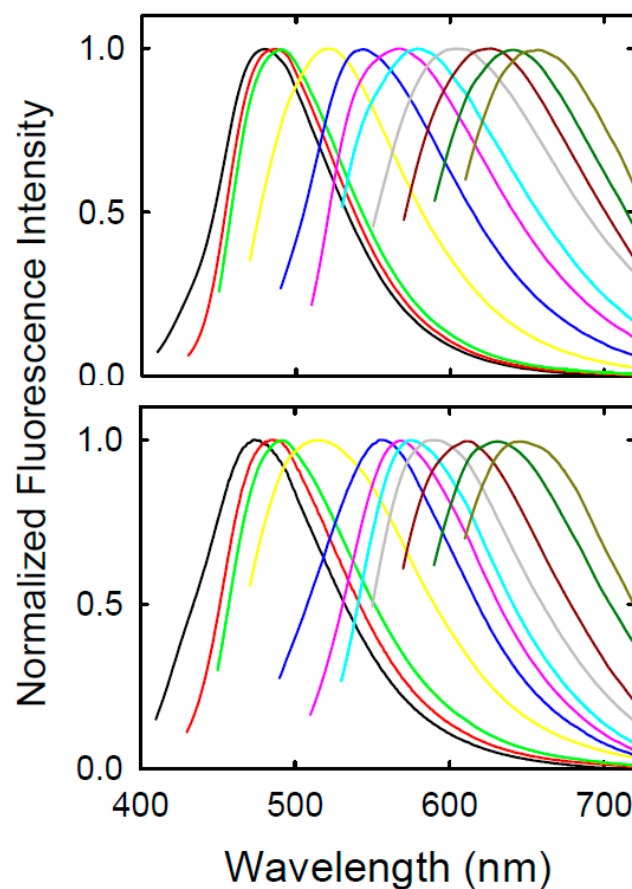


Figure 4. The excitation wavelength dependence of fluorescence emissions for CS330 (upper) and CS_{MT} (lower) in aqueous solutions, with the excitations of 400 nm and (from left to right) in 20 nm increments (thus 600 nm excitation for the last spectrum at right).

The structural and morphological characteristics of the three PEI/CA samples were probed by atomic force microscopy (AFM) imaging. According to the AFM images shown in Figure 7, the CS200 sample is apparently composed of smaller nano-carbon domains in lower population, consistent with the consequence of insufficient carbonization due to the much-too-mild thermal processing conditions for the sample. The CS330 sample contains more defined nano-carbon domains, with features somewhat similar to those found in the AFM image of PEI-CDots derived from preexisting small-carbon nanoparticles (Supplementary Materials). The CS_{MT} sample seems morphologically different from the other two samples (Figure 7). However, the sample characteristics revealed in AFM images may not be sufficient to explain the observed different photoinduced antibacterial activities, though not contradictory to the observed behaviors of the samples either. Further, an unfortunate consequence of the results is that they may serve to disqualify AFM from being a viable tool for more quantitative probing and understanding of the structural and morphological details in these PEI/CA samples. One may naturally suggest high-resolution transmission electron microscopy (HR-TEM) for the task, but the reality is that HR-TEM is intrinsically unsuitable for the probing of these soft composite-like materials on their structures and morphologies at the length scale (or resolution) of sub-nanometer to a few nanometers.

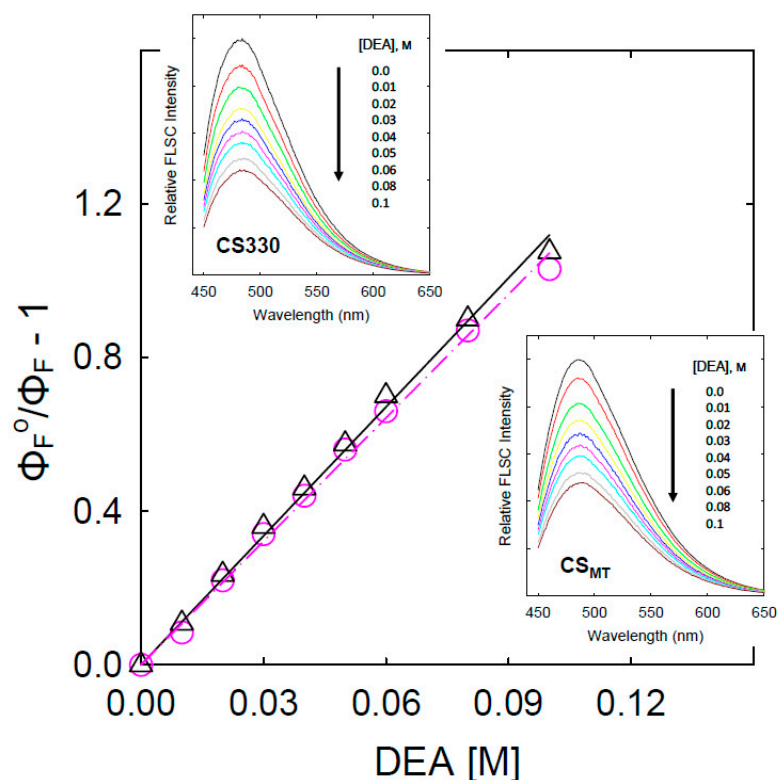


Figure 5. Stern–Volmer plots for the quenching of fluorescence emission intensity by DEA for CS330 (triangle, solid line) and CS_{MT} (circle, dash-dot line) in ethanol solutions, with the slopes (Stern–Volmer constants) of 11.2 M⁻¹ and 10.7 M⁻¹, respectively. Insets: The corresponding fluorescence emission spectra with the quenching at different DEA concentrations.

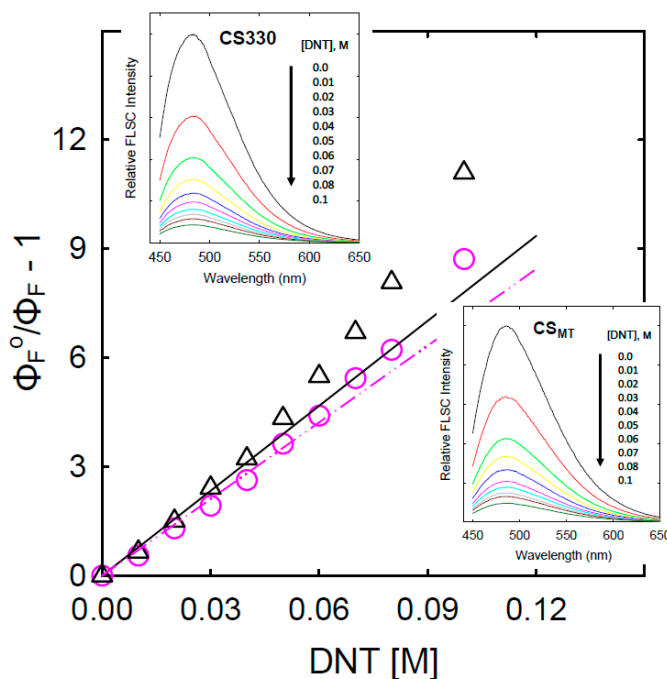


Figure 6. Stern–Volmer plots for the quenching of fluorescence emission intensity by DNT for CS330 (triangle, solid line) and CS_{MT} (circle, dash-dot-dot line) in ethanol solutions, with the slopes (Stern–Volmer constants for the linear portion with low DNT concentrations) of 79 M⁻¹ and 70 M⁻¹, respectively. Insets: The corresponding fluorescence emission spectra with the quenching at different DNT concentrations.

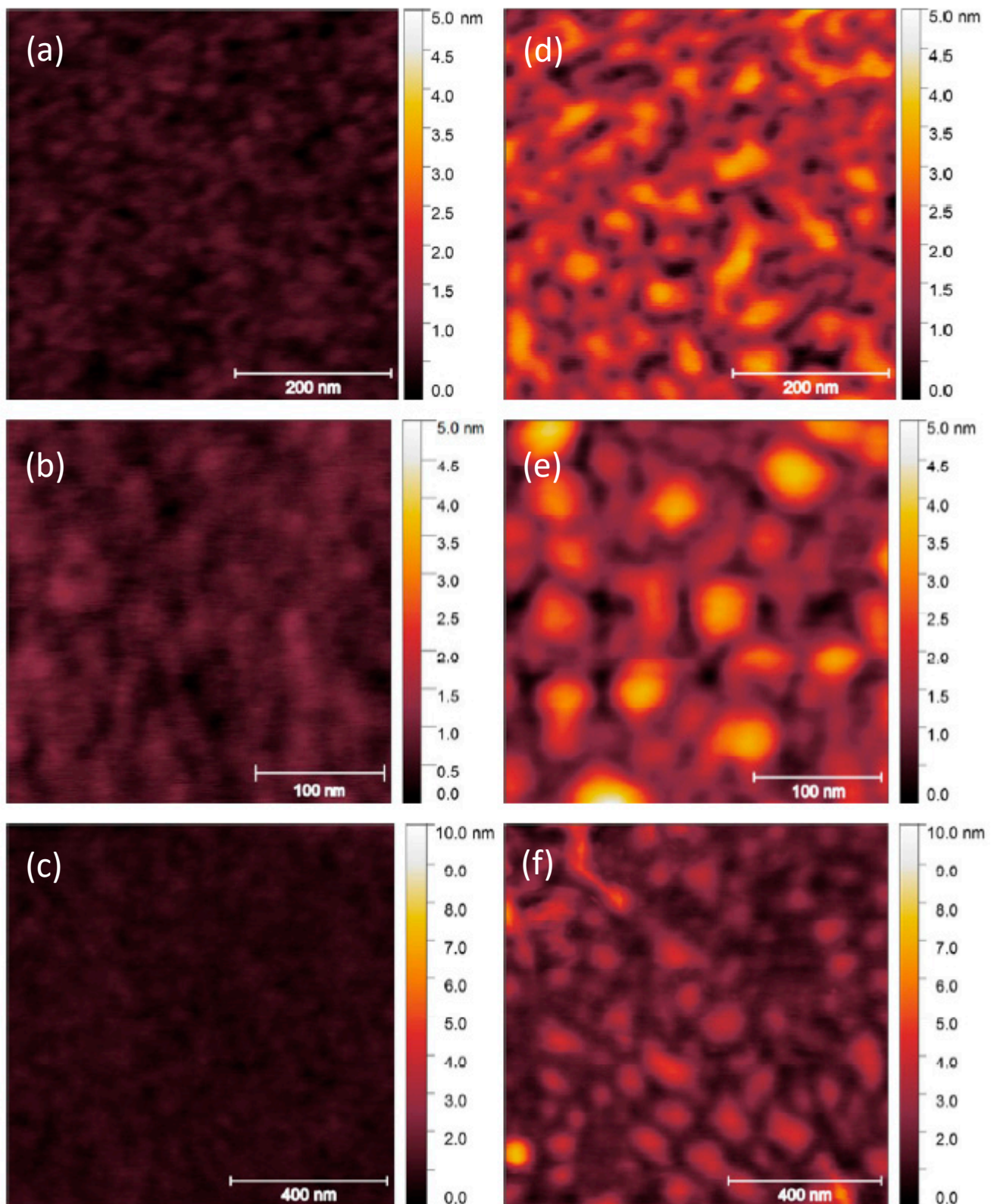


Figure 7. AFM images of the CS200 (d), CS330 (e), and CSMT (f) samples on Si wafers, with the corresponding images of clean Si wafers on the left (a–c).

Mechanistically, the optical absorptions of all these samples over the visible spectrum must be due to electronic transitions in the small-carbon nanoparticles or, analogously, the nano-carbon domains. There is experimental evidence for the insensitive nature of

the absorptions to the surface organic functionalization of the small-carbon nanoparticles in CDots [1,36]. The same is likely applicable to the absorptions of the carbonization-produced samples, in which the nano-carbon domains are immersed in various organic materials (Figure 1). In the classically defined CDots derived from preexisting small-carbon nanoparticles, upon photoexcitation, there must be rapid charge transfers and separation for the generation of separated electrons and holes that are trapped at abundant surface defect sites of the small-carbon nanoparticles (Figure 8) [1]. The difference between “naked” small-carbon nanoparticles and their surface functionalized counterpart CDots must be such that in the latter, the effective stabilization of the surface defect sites is made possible by the organic functionalization, a phenomenon almost identical to that well established for conventional semiconductor quantum dots (QDs, CdSe nanoparticles, for example) in their early development [43,44]. The radiative recombinations of the separated redox pairs in CDots are responsible for the observed bright and colorful fluorescence emissions (Figure 8), with experimentally determined quantum yields orders of magnitude higher than those of solvent-dispersed small-carbon nanoparticles [1,45]. Such a photoexcited state mechanistic framework may also be considered for the observed spectroscopic properties of the carbonization-produced samples.

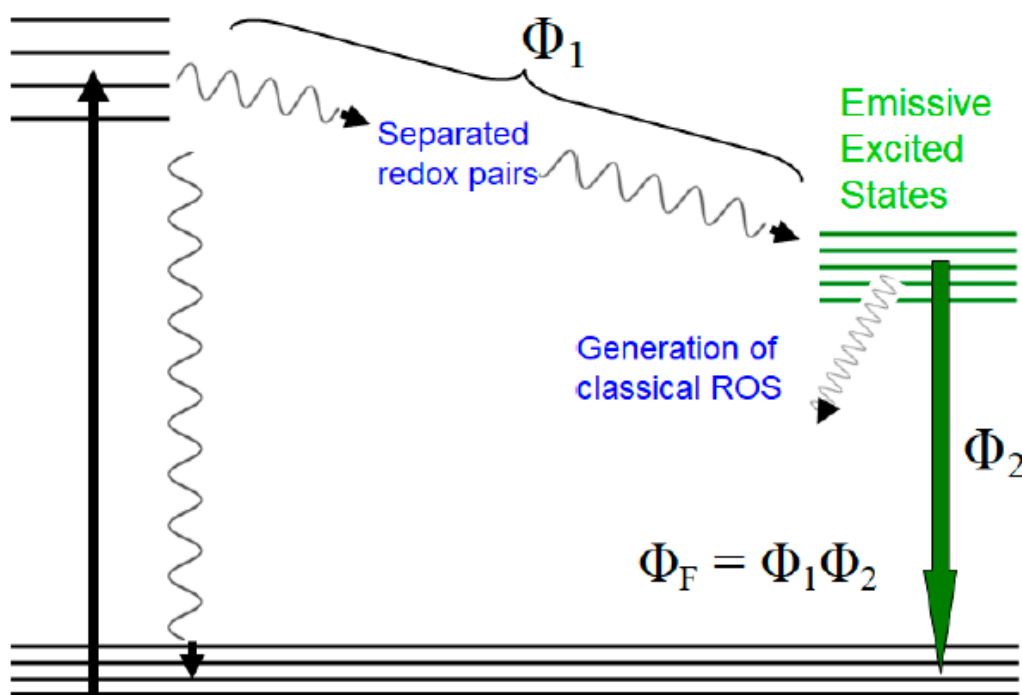


Figure 8. A state energy diagram on the photoexcited states and processes of CDots, highlighting the two sets of highly reactive species: the separated redox pairs from the initial charge transfers and separation and the generation of classical ROS as a part of the nonradiative deactivation of the emissive excited states. Φ_F denotes observed fluorescence quantum yields (reprinted with permission from [40]. Copyright 2020 Elsevier).

The three PEI/CA samples were from the same precursor mixture and thermal carbonization, but with different processing conditions, thus, the logical expectation that they should all be mixtures of nano-carbon (namely non-molecular carbon produced in the thermal carbonization) and organic species (precursor molecules crosslinked in the thermal processing with or without involving the nano-carbon) in different compositions and structural arrangements. As suggested previously [19], samples of such mixtures are more appropriately considered and denoted as “nano-carbon/organic hybrids” (Figure 1). Locally, in the structure of these hybrids, the configuration of a nano-carbon domain immersed in the matrix of organic species might be effectively analogous or equivalent to a small-

carbon nanoparticle with surface passivation by the organic functionalization in classically defined CDots (Figure 1) [19]. Such an equivalency might account for the observed similar fluorescence emission properties of the hybrids and CDots. Nevertheless, the composition of the CS200 sample is too low in nano-carbon content due to the much-too-mild thermal processing conditions in the synthesis, likely only marginally capable of the properties dominated by the passivated nano-carbon domains found in the other hybrids. Despite the equivalency argument that would place the hybrids and classically defined CDots under the same mechanistic umbrella, the photoinduced antibacterial activities of the hybrids (Figure 3) obviously diverge from the optical spectroscopic properties, not only in terms of the comparison with PEI-CDots but also for the very different antibacterial outcomes between the CS330 and CD_{MT} samples.

In the same mechanistic framework discussed above for the photoexcited state properties and processes of CDots (Figure 8), the related photoinduced antimicrobial function can be attributed to the combined actions by two sets of reactive species, the separated redox pairs formed upon photoexcitation and the classical reactive oxygen species (ROS) produced in the emissive excited states (Figure 8) [40]. The former is analogous to the “light-activated redox species” (LARS) proposed for conventional semiconductor QDs in the mechanistic account for their photoinduced antimicrobial properties [46] and the latter is equivalent to the ROS generated by classical molecular dye photosensitizers [47,48]. In this regard, one might argue that these same reactive species could also be found in the photoexcited “nano-carbon/organic hybrids” (Figure 1), in light of the above discussed equivalency of their local structural configuration to that of classically defined CDots, so that the same or similar photoinduced antibacterial function should be expected. Nevertheless, a counter argument is that the formation of the reactive species may not be equivalent to the realization of their reactive function, which would depend significantly on the interactions of the reactive species with the targeted bacteria. The fact of the matter is that the reactive species are, by nature, short lived, especially so for the separated redox pairs, thus, requiring close-range actions against the bacterial cells [40]. The structural and morphological characteristics of the hybrids, with the nano-carbon domains as the centers for the photoinduced generation of reactive species immersed in the matrix of abundant organic species, must be unfavorable to the required close-range (or near-neighbor) antibacterial action in general (versus PEI-CDots, for example, Figure 3) or practically impossible for the CS_{MT} and CS200 samples (Figure 3) in particular.

In summary, the dot samples prepared by the thermal processing of selected organic precursors, if the processing conditions are adequate for the intended carbonization, may be considered and denoted as “nano-carbon/organic hybrids” for their sample structures, characterized by nano-carbon domains in crosslinked mixtures with abundant organic species. In the hybrids, there may be nanoscale structural features, specifically individual nano-carbon domains immersed in organic matrices for the effect similar to passivation, which are analogous or equivalent to the organic functionalization of pre-existing small-carbon nanoparticles in the classically defined CDots. Such structural features of the hybrids make their optical spectroscopic properties comparable to those of the classically defined CDots. For the photoinduced antimicrobial function associated with the same photoexcited state properties and processes, the sample structural and morphological characteristics of the hybrids may hinder the required close-range or near-neighbor action (due to the short-lived nature of the reactive species) against the targeted bacteria, resulting in poor outcomes or no activities at all.

Supplementary Materials: The following supporting information can be downloaded at: <https://www.mdpi.com/article/10.3390/c8040054/s1>. Details on the preparation and characterization of PEI-CDots. Figure S1: Representative AFM image for PEI-CDots. Figure S2: Representative TEM imaging results for PEI-CDots. Figure S3: Absorption spectrum of PEI-CDots in aqueous solution (solid line) is compared with that of the aqueous dispersed small carbon nanoparticles (dash-dot-dot line). Inset: Fluorescence spectra of PEI-CDots at different excitation wavelengths (from left to right with excitation at 400 nm and in 20 nm increments).

Author Contributions: Data acquisition and analyses, A.F.A., P.W., E.Y.C., L.G., Y.T., I.S.F., F.S.A.S., L.P. and W.C.; Funding acquisition, L.Y., Y.T. and Y.-P.S.; Investigation, A.F.A., P.W., E.Y.C. and L.G.; Project administration, L.Y., C.E.B. and Y.-P.S.; Supervision, L.Y., C.E.B. and Y.-P.S.; Validation, A.F.A., P.W. and E.Y.C.; Writing—original draft, L.Y., C.E.B. and Y.-P.S.; Writing—review and editing, L.Y., C.E.B. and Y.-P.S. All authors have read and agreed to the published version of the manuscript.

Funding: National Science Foundation, USDA, and Air Force Research Laboratory.

Data Availability Statement: All data is contained within the article or Supplementary Material.

Acknowledgments: Financial support from NSF (2102021 and 2102056, and 1855905), USDA (2019-67018-29689), and Air Force Research Laboratory is gratefully acknowledged. L.P. and W.C. were participants in the Palmetto Academy, a summer undergraduate research program of the South Carolina Space Grant Consortium.

Conflicts of Interest: The authors declare no conflict of interest.

References

1. Sun, Y.-P. *Carbon Dots—Exploring Carbon at Zero-Dimension*; Springer International Publishing: Berlin/Heidelberg, Germany, 2020.
2. Sun, Y.-P.; Zhou, B.; Lin, Y.; Wang, W.; Fernando, K.A.S.; Pathak, P.; Meziani, M.J.; Harruff, B.A.; Wang, X.; Wang, H.; et al. Quantum-Sized Carbon Dots for Bright and Colorful Photoluminescence. *J. Am. Chem. Soc.* **2006**, *128*, 7756–7757. [[CrossRef](#)] [[PubMed](#)]
3. Sun, Y.-P. Fluorescent Carbon Nanoparticles. U.S. Patent 7,829,772, 9 November 2010.
4. Cao, L.; Meziani, M.J.; Sahu, S.; Sun, Y.-P. Photoluminescence Properties of Graphene *versus* Other Carbon Nanomaterials. *Acc. Chem. Res.* **2013**, *46*, 171–180. [[CrossRef](#)] [[PubMed](#)]
5. Luo, P.G.; Sahu, S.; Yang, S.-T.; Sonkar, S.K.; Wang, J.; Wang, H.; LeCroy, G.E.; Cao, L.; Sun, Y.-P. Carbon “Quantum” Dots for Optical Bioimaging. *J. Mater. Chem. B* **2013**, *1*, 2116–2127. [[CrossRef](#)] [[PubMed](#)]
6. Ding, C.; Zhu, A.; Tian, Y. Functional Surface Engineering of C-Dots for Fluorescent Biosensing and in Vivo Bioimaging. *Acc. Chem. Res.* **2014**, *47*, 20–30. [[CrossRef](#)]
7. Luo, P.G.; Yang, F.; Yang, S.-T.; Sonkar, S.K.; Yang, L.; Broglie, J.J.; Liu, Y.; Sun, Y.-P. Carbon-Based Quantum Dots for Fluorescence Imaging of Cells and Tissues. *RSC Adv.* **2014**, *4*, 10791–10807. [[CrossRef](#)]
8. Lim, S.Y.; Shen, W.; Gao, Z. Carbon Quantum Dots and Their Applications. *Chem. Soc. Rev.* **2015**, *44*, 362–381. [[CrossRef](#)]
9. Fernando, K.A.S.; Sahu, S.; Liu, Y.; Lewis, W.K.; Gulians, E.A.; Jafariyan, A.; Wang, P.; Bunker, C.E.; Sun, Y.-P. Carbon Quantum Dots and Applications in Photocatalytic Energy Conversion. *ACS Appl. Mater. Interfaces* **2015**, *7*, 8363–8376. [[CrossRef](#)]
10. LeCroy, G.E.; Yang, S.-T.; Yang, F.; Liu, Y.; Fernando, K.A.S.; Bunker, C.E.; Hu, Y.; Luo, P.G.; Sun, Y.-P. Functionalized Carbon Nanoparticles: Syntheses and Applications in Optical Bioimaging and Energy Conversion. *Coord. Chem. Rev.* **2016**, *320*, 66–81. [[CrossRef](#)]
11. Peng, Z.; Han, X.; Li, S.; Al-Youbi, A.O.; Bashammakh, A.S.; El-Shahawi, M.S.; Leblanc, R.M. Carbon Dots: Biomacromolecule Interaction, Bioimaging and Nanomedicine. *Coord. Chem. Rev.* **2017**, *343*, 256–277. [[CrossRef](#)]
12. Hutton, G.A.M.; Martindale, B.C.M.; Reisner, E. Carbon Dots as Photosensitisers for Solar-Driven Catalysis. *Chem. Soc. Rev.* **2017**, *46*, 6111–6123. [[CrossRef](#)]
13. Xu, D.; Lin, Q.; Chang, H.-T. Recent Advances and Sensing Applications of Carbon Dots. *Small Methods* **2020**, *4*, 1900387. [[CrossRef](#)]
14. Das, R.; Bandyopadhyay, R.; Pramanik, P. Carbon Quantum Dots from Natural Resource: A Review. *Mater. Today Chem.* **2018**, *8*, 96–109. [[CrossRef](#)]
15. Du, J.; Xu, N.; Fan, J.; Sun, W.; Peng, X. Carbon Dots for In Vivo Bioimaging and Theranostics. *Small* **2019**, *15*, 1805087. [[CrossRef](#)]
16. Li, Y.; Xu, X.; Wu, Y.; Zhuang, J.; Zhang, X.; Zhang, H.; Lei, B.; Hu, C.; Liu, Y. A Review on the Effects of Carbon Dots in Plant Systems. *Mater. Chem. Front.* **2020**, *4*, 437–448. [[CrossRef](#)]
17. Indriyati; Primadona, I.; Permatasari, F.A.A.; Irham, M.A.; Nasir, D.E.M.; Iskandar, F. Recent Advances and Rational Design Strategies of Carbon Dots towards Highly Efficient Solar Evaporation. *Nanoscale* **2021**, *13*, 7523–7532. [[CrossRef](#)]
18. Đorđević, L.; Arcudi, F.; Cacioppo, M.; Prato, M.A. Multifunctional Chemical Toolbox to Engineer Carbon Dots for Biomedical and Energy Applications. *Nat. Nanotech.* **2022**, *17*, 112–130. [[CrossRef](#)] [[PubMed](#)]
19. Yuan, D.; Wang, P.; Yang, L.; Quimby, J.L.; Sun, Y.-P. Carbon “Quantum” Dots for Bioapplications. *Exp. Bio. Med.* **2022**, *247*, 300–309. [[CrossRef](#)]
20. Dong, Y.; Wang, R.; Li, G.; Chen, C.; Chi, Y.; Chen, G. Polyamine-Functionalized Carbon Quantum Dots as Fluorescent Probes for Selective and Sensitive Detection of Copper Ions. *Anal. Chem.* **2012**, *84*, 6220–6224. [[CrossRef](#)]
21. Dong, Y.; Wang, R.; Li, H.; Shao, J.; Chi, Y.; Lin, X.; Chen, G. Polyamine-Functionalized Carbon Quantum Dots for Chemical Sensing. *Carbon* **2012**, *50*, 2810–2815. [[CrossRef](#)]
22. Wang, R.; Li, G.; Dong, Y.; Chi, Y.; Chen, G. Carbon Quantum Dot-Functionalized Aerogels for NO₂ Gas Sensing. *Anal. Chem.* **2013**, *85*, 8065–8069. [[CrossRef](#)]

23. Dong, Y.; Wang, R.; Tian, W.; Chi, Y.; Chen, G. “Turn-on” Fluorescent Detection of Cyanide Based on Polyamine-Functionalized Carbon Quantum Dots. *RSC Adv.* **2014**, *4*, 3685–3689. [[CrossRef](#)]
24. Liu, J.; Liu, X.; Luo, H.; Gao, Y. One-Step Preparation of Nitrogen-Doped and Surface-Passivated Carbon Quantum Dots with High Quantum Yield and Excellent Optical Properties. *RSC Adv.* **2014**, *4*, 7648. [[CrossRef](#)]
25. Wang, C.; Xu, Z.; Zhang, C. Polyethyleneimine-Functionalized Fluorescent Carbon Dots: Water Stability, PH Sensing, and Cellular Imaging. *ChemNanoMat* **2015**, *1*, 122–127. [[CrossRef](#)]
26. Pierrat, P.; Wang, R.; Kereselidze, D.; Lux, M.; Didier, P.; Kichler, A.; Pons, F.; Lebeau, L. Efficient in Vitro and in Vivo Pulmonary Delivery of Nucleic Acid by Carbon Dot-Based Nanocarriers. *Biomaterials* **2015**, *51*, 290–302. [[CrossRef](#)] [[PubMed](#)]
27. Hou, X.; Hu, Y.; Wang, P.; Yang, L.; Al Awak, M.M.; Tang, Y.; Twara, F.K.; Qian, H.; Sun, Y.-P. Modified Facile Synthesis for Quantitatively Fluorescent Carbon Dots. *Carbon* **2017**, *122*, 389–394. [[CrossRef](#)]
28. Wang, P.; Meziani, M.J.; Fu, Y.; Bunker, C.E.; Hou, X.; Yang, L.; Msellek, H.; Zaharias, M.; Darby, J.P.; Sun, Y.-P. Carbon Dots versus Nano-Carbon/Organic Hybrids—Dramatically Different Behaviors in Fluorescence Sensing of Metal Cations with Structural and Mechanistic Implications. *Nanoscale Adv.* **2021**, *3*, 2316–2324. [[CrossRef](#)]
29. Khan, S.; Sharma, A.; Ghoshal, S.; Jain, S.; Hazra, M.K.; Nandi, C.K. Small Molecular Organic Nanocrystals Resemble Carbon Nanodots in Terms of Their Properties. *Chem. Sci.* **2018**, *9*, 175–180. [[CrossRef](#)]
30. Hinterberger, V.; Damm, C.; Haines, P.; Guldi, D.M.; Peukert, W. Purification and Structural Elucidation of Carbon Dots by Column Chromatography. *Nanoscale* **2019**, *11*, 8464–8474. [[CrossRef](#)]
31. Liang, W.; Ge, L.; Hou, X.; Ren, X.; Yang, L.; Bunker, C.E.; Overton, C.M.; Wang, P.; Sun, Y.-P. Evaluation of Commercial “Carbon Quantum Dots” Sample on Origins of Red Absorption and Emission Features. *C J. Carbon Res.* **2019**, *5*, 70. [[CrossRef](#)]
32. Liang, W.; Wang, P.; Meziani, M.J.; Ge, L.; Yang, L.; Patel, A.K.; Morgan, S.O.; Sun, Y.-P. On the Myth of “Red/Near-IR Carbon Quantum Dots” from Thermal Processing of Specific Colorless Organic Precursors. *Nanoscale Adv.* **2021**, *3*, 4186–4195. [[CrossRef](#)]
33. Liang, W.; Wang, P.; Yang, L.; Overton, C.M.; Hewitt, B.; Sun, Y.-P. Chemical Reactions in Thermal Carbonization Processing of Citric Acid—Urea Mixtures. *Gen. Chem.* **2021**, *7*, 210011–210017.
34. Bartolomei, B.; Bogo, A.; Amato, F.; Ragazzon, G.; Prato, M. Nuclear Magnetic Resonance Reveals Molecular Species in Carbon Nanodot Samples Disclosing Flaws. *Angew. Chem. Int. Ed.* **2022**, *61*, e202200038. [[CrossRef](#)] [[PubMed](#)]
35. Hu, Y.; Al Awak, M.M.; Yang, F.; Yan, S.; Xiong, Q.; Wang, P.; Tang, Y.; Yang, L.; LeCroy, G.E.; Bunker, C.E.; et al. Photoexcited State Properties of Carbon Dots from Thermally Induced Functionalization of Carbon Nanoparticles. *J. Mater. Chem. C* **2016**, *4*, 10554–10561. [[CrossRef](#)]
36. Ge, L.; Pan, N.; Jin, J.; Wang, P.; LeCroy, G.E.; Liang, W.; Yang, L.; Teisl, L.R.; Tang, Y.; Sun, Y.-P. Systematic Comparison of Carbon Dots from Different Preparations—Consistent Optical Properties and Photoinduced Redox Characteristics in Visible Spectrum, and Structural and Mechanistic Implications. *J. Phys. Chem. C* **2018**, *122*, 21667–21676. [[CrossRef](#)]
37. Meziani, M.J.; Dong, X.; Zhu, L.; Jones, L.P.; LeCroy, G.E.; Yang, F.; Wang, S.; Wang, P.; Zhao, Y.; Yang, L.; et al. Visible-Light-Activated Bactericidal Functions of Carbon “Quantum” Dots. *ACS Appl. Mater. Interfaces* **2016**, *8*, 10761–10766. [[CrossRef](#)] [[PubMed](#)]
38. Dong, X.; Liang, W.; Meziani, M.J.; Sun, Y.-P.; Yang, L. Carbon Dots as Potent Antimicrobial Agents. *Theranostics* **2020**, *10*, 671–686. [[CrossRef](#)] [[PubMed](#)]
39. Abu Rabe, D.I.; Mohammed, O.O.; Dong, X.; Patel, A.K.; Overton, C.M.; Tang, Y.; Kathariou, S.; Sun, Y.-P.; Yang, L. Carbon Dots for Highly Effective Photodynamic Inactivation of Multidrug-Resistant Bacteria. *Mater. Adv.* **2020**, *1*, 321–325. [[CrossRef](#)]
40. Dong, X.; Ge, L.; Abu Rabe, D.I.; Mohammed, O.O.; Wang, P.; Tang, Y.; Kathariou, S.; Yang, L.; Sun, Y.-P. Photoexcited State Properties and Antibacterial Activities of Carbon Dots Relevant to Mechanistic Features and Implications. *Carbon* **2020**, *170*, 137–145. [[CrossRef](#)]
41. LeCroy, G.E.; Messina, F.; Sciortino, A.; Bunker, C.E.; Wang, P.; Fernando, K.A.S.; Sun, Y.-P. Characteristic Excitation Wavelength Dependence of Fluorescence Emissions in Carbon “Quantum” Dots. *J. Phys. Chem. C* **2017**, *121*, 28180–28186. [[CrossRef](#)]
42. LeCroy, G.E.; Fernando, K.A.S.; Bunker, C.E.; Wang, P.; Tomlinson, N.; Sun, Y.-P. Steady-State and Time-Resolved Fluorescence Studies on Interactions of Carbon “Quantum” Dots with Nitrotoluenes. *Inorg. Chim. Acta* **2017**, *468*, 300–307. [[CrossRef](#)]
43. Kortan, A.R.; Hull, R.; Opila, R.L.; Bawendi, M.G.; Steigerwald, M.L.; Carroll, P.J.; Brus, L.E. Nucleation and Growth of CdSe on ZnS Quantum Crystallite Seeds, and Vice Versa, in Inverse Micelle Media. *J. Am. Chem. Soc.* **1990**, *112*, 1327–1332. [[CrossRef](#)]
44. Murray, C.B.; Norris, D.J.; Bawendi, M.G. Synthesis and Characterization of Nearly Monodisperse CdE (E = sulfur, selenium, tellurium) Semiconductor Nanocrystallites. *J. Am. Chem. Soc.* **1993**, *115*, 8706–8715. [[CrossRef](#)]
45. Cao, L.; Anilkumar, P.; Wang, X.; Liu, J.-H.; Sahu, S.; Meziani, M.J.; Myers, E.; Sun, Y.-P. Reverse Stern-Volmer Behavior for Luminescence Quenching in Carbon Nanoparticles. *Can. J. Chem.* **2011**, *89*, 104–109. [[CrossRef](#)]
46. Courtney, C.M.; Goodman, S.M.; McDaniel, J.A.; Madinger, N.E.; Chatterjee, A.; Nagpal, P. Photoexcited Quantum Dots for Killing Multidrug-Resistant Bacteria. *Nat. Mater.* **2016**, *15*, 529–534. [[CrossRef](#)]
47. Hara, K.; Holland, S.; Woo, J. Effects of Exogenous Reactive Oxygen Species Scavengers on the Survival of Escherichia coli B23 during Exposure to UV-A Radiation. *J. Exp. Microbiol. Immunol.* **2004**, *12*, 62–66.
48. Ishiyama, K.; Nakamura, K.; Ikai, H.; Kanno, T.; Kohno, M.; Sasaki, K.; Niwano, Y. Bactericidal Action of Photogenerated Singlet Oxygen from Photosensitizers Used in Plaque Disclosing Agents. *PLoS ONE* **2012**, *7*, e37871. [[CrossRef](#)] [[PubMed](#)]